Civil Engineering and Applied Solutions

Research Article

journal homepage: ceas.journals.umz.ac.ir

CEAS Civil Engineering and Applied Solutions

A Hybrid CFD–Machine Learning Framework for Modeling Discharge Hysteresis in Twin Circular Culverts

Ehsan Behnamtalab [a*], Mohsen Behnamtalab [b]

[a] *Department of Engineering, Civil Engineering Group, Hakim Sabzevari University, Sabzevar, Iran*
[b] *Civil Engineering Department, Sharif University of Technology, Tehran, Iran*

ARTICLE INFO

Article history:

Received 18 February 2026

Revised 26 March 2026

Accepted 03 June 2026

Available online 01 January 2027

Keywords:

Twin culvert

Head-Discharge

Numerical simulation

Machine learning

RANS

ABSTRACT

This study investigates the hydraulic behavior of twin circular culverts under unsteady flow, considering rising and receding inlet flows and varying upstream water levels. Three-dimensional numerical simulations were conducted using RANS equations with the RNG k–ε turbulence model and validated against laboratory data, showing excellent agreement. Results indicate that through-flow discharge remains nearly constant across rising and receding phases, while overtopping flow exhibits significant differences (~22%). Outflow during recession is approximately 1.5 times higher than during the rising stage. Complementary data-driven modeling using eight machine learning algorithms, including Gradient Boosting, AdaBoost, Random Forest, and Neural Networks, demonstrated high accuracy in predicting nonlinear discharge–head relationships, with R^2 up to 0.992 for numerical and 0.985 for experimental data. Models performed better during receding phases due to more stable flow conditions. The integration of CFD simulations and machine learning provides detailed flow insights and rapid, accurate discharge estimation, offering a reliable framework for culvert design, flow assessment, and hydraulic optimization under complex unsteady conditions.

How to cite this article: Behnamtalab, E., Behnamtalab, M. A Hybrid CFD–Machine Learning Framework for Modeling Discharge Hysteresis in Twin Circular Culverts. Civil Engineering and Applied Solutions. 2027; 3(1): 117–130. doi:10.22080/ceas.2026.31318.1079.

1. Introduction

Drainage systems along highways and railways are designed to convey surface water and prevent upstream flooding, with culverts being a primary component. Compared to bridges, culverts are more cost-effective initially, require precise hydraulic design, and depend on backfill quality for structural strength, though their maintenance costs can be higher [1]. Culverts are typically designed based on historical rainfall records to estimate discharge rates. However, with the substantial changes in precipitation patterns driven by global warming, there is an increased likelihood of future flood disasters due to undersized and poorly designed culverts [2-5]. Recent flood events have emphasized the vital role of culverts in safely conveying surface water beneath roads, railways, and dams. Proper design, construction, and maintenance are crucial, as culverts protect channels and embankments and ensure long-term structural performance.

In recent years, many researchers have investigated different aspects and behaviors of culvers. In a study, researchers analyzed vertical earth pressure on Hinged Prefabricated Box Culverts (HPBC) using field tests and FLAC3D simulations, comparing them

* Corresponding author.
E-mail addresses: e.behnamtalab@hsu.ac.ir (E. Behnamtalab).

https://doi.org/10.22080/ceas.2026.31318.1079
ISSN: 3092-7749/

with Monolithic Box Culverts (MBC). They proposed a modified calculation method that improved the accuracy of vertical pressure estimation beyond existing AASHTO and Chinese design codes [6]. A Decision Tree–SMOTE framework was developed to predict culvert conditions and prioritize inspections. Applied to 12,400 culverts, it achieved high accuracy and reduced inspections by 44% [7]. In a study, a comprehensive review of local scour downstream of culverts emphasized the influence of flow regime, sediment properties, and geometric factors. The study highlighted that incorporating these parameters into culvert design is crucial for enhancing structural safety and long-term durability [8]. In another study, a physical modeling study compared scour development at box and circular culvert outlets under varying blockage ratios and flow conditions. Results showed that circular culverts caused greater scour, and scour depth increased with discharge, providing useful insights for optimizing culvert outlet design. [9].

Culverts are available in various geometric shapes, with rectangular and circular types being the most common. The most suitable culvert design is the culvert that can pass the design flow well with the lowest cost. Many researches have been done regarding the design method and different flow conditions in culverts, among which it can refer to the studies of Dasika [10], Montes and Dasika [11], Hager and Giudice [12], Johnson and Brown [13] and Ansar et al. [14]. Most of these studies demonstrated significant differences in discharge behavior between the rising and falling limbs of the hydrograph, attributable to varying flow conditions during culvert filling and draining phases. Lee and Jin [15] created a computer program for designing rectangular culverts, which requires multiple iterations to reach a final solution. Ku and Jun [16] developed a computational tool that integrates non-uniform flow characteristics in culverts by comprehensively incorporating updated data from the FHWA. Richmond et al. [17] investigated the impact of velocity distributions across cross sections within a corrugated culvert barrel on juvenile fish migration, emphasizing ecological considerations in culvert design.

Although culverts are straightforward to construct, their hydraulic design is inherently complex and influenced by multiple factors. The flow cannot always be classified strictly as pressurized or free flow; in some cases, it represents a combination of both regimes [18]. Chow [19] classified the flow inside the culvert into six hydraulic types. The upstream water depth, the height of the culvert, the water depth inside the culvert, the length and slope of the culvert are the factors that determine the type of flow inside the culvert. Yoo and Lee [20] stated that the classification of flow in a culvert is expressed according to three characteristics. The first characteristic is whether the culvert inlet flow is submerged or not, which is determined by the upstream water level. The second characteristic includes the characteristics of the flow regime inside the channel, and the third characteristic is the flow condition downstream of the culvert. Culvert design is generally based on the flood discharge corresponding to a specified return period, which varies according to regional and climatic conditions. Kang et al. [21] suggested that the concept of critical storm duration is appropriate for estimating design flood discharge in culvert design. The preliminary and optimal design involves a submerged inlet operating with near-full flow conditions, ensuring supercritical flow and maximizing channel capacity [22].

Hydraulically optimized designs have had limited impact on culvert practice, as guidelines focus on pipe sizing but offer little advice on materials, wing wall angles, or slopes. Consequently, inefficient designs like square inlets or high-friction barrels remain common, with HDS-5 from the FHWA being one of the most comprehensive references [23]. The equations presented in HDS-5 are based on the Bernoulli equation, modified in accordance with experimental findings from studies conducted during the 1950s and 1960s [24-29]. Culvert flow is classified into inlet control (IC) and outlet control (OC) based on hydraulic theory. Experimental studies using HEC-RAS and HY-8 showed that culvert length and roughness significantly affect performance, with HY-8 performing better under rough-bed conditions and no clear advantage for bridge hydraulics. [30].

Under inlet control, the flow is solely limited by the size, shape, and configuration of the inlet. The sudden reduction in cross-sectional flow area at the inlet, where an open channel enters the culvert, causes head loss [31]. The culvert barrel may still convey higher flow rates and therefore does not limit the flow. In these situations, culvert flows are treated as weir (unsubmerged) or orifice (submerged) flows. The flow rate, cross-sectional area, shape, and inlet configuration of the culvert determine the headwater height under inlet control. Under outlet-control conditions, head loss is influenced not only by inlet parameters but also by culvert length, material, and tailwater depth, making the barrel a key factor in determining overall flow capacity [23]. Under submerged-inlet conditions, culverts behave like orifices with air recirculation limiting the effective flow area. Full submergence at the outlet displaces all air, fills the cross-section, and causes a transition from open-channel to pressurized flow conditions [10].

In parallel to traditional methods, Machine Learning (ML) has emerged as a transformative tool in water resources engineering, demonstrated by its use in developing efficient surrogate models for complex flow simulations [32], predicting scour depth at coastal structures with over 80% accuracy using ensemble methods [33]and deriving compact design equations for spillways via gene expression programming [34]. In addition, hybrid and soft computing approaches have been widely applied in civil engineering problems; for example, [35] developed a hybrid ANFIS-based framework for predicting pipe failure rates, showing that combining multiple models can significantly improve predictive accuracy. Similarly, Tabari and Sanayei [36] employed artificial neural networks and support vector regression for predicting dam crest displacement, highlighting the effectiveness of data-driven models in capturing complex structural responses. Subsequently, deep learning architectures like CNNs and LSTMs have enhanced the modeling of spatiotemporal hydrologic systems [37] and improved urban drainage management through real-time flood prediction and pipe defect detection [38], with notable success in culvert blockage detection achieving 94% accuracy [39]. More recently, reinforcement learning techniques have also been introduced for adaptive water resources management; for instance, Masoumi et al. [40] demonstrated the effectiveness of Q-learning in optimizing reservoir operations under dynamic and uncertain conditions. The most significant advancement is the integration of physical principles into physics-informed ML models, which has substantially improved the reliability and speed of CFD simulations [41] and coastal hazard forecasting Židek et al. [42], marking a shift towards more robust, physics-conscious predictive tools.

Despite the significant progress in both numerical modeling and machine learning applications in hydraulic engineering, most studies have treated these approaches separately. The proposed hybrid framework leverages the strengths of both approaches: CFD provides a detailed physical representation of flow behavior, while machine learning enables rapid prediction with significantly reduced computational cost. This combination offers improved accuracy and practical utility compared to traditional empirical or purely numerical methods.

Considering the above-mentioned factors and previous research gaps, this study employs numerical simulations to investigate the turbulent flow characteristics of twin circular culverts. Also, the receding and rising inlet flow to culverts and the upstream water level change rate are parameters that have been investigated in this research. Moreover, this research evaluates numerically the discharge passing through the culverts and the overtopping flow.

2. Governing equations

This study employs the Reynolds-Averaged Navier-Stokes (RANS) equations to simulate turbulent flow. The RANS equations represent the time-averaged conservation of momentum and mass for turbulent, incompressible Newtonian fluids [43-45]. The continuity and momentum equations are:

$$\frac{\partial u_i}{\partial x_i} = 0 \tag{1}$$

$$\frac{\partial u_i}{\partial t} + u_i \frac{\partial u_j}{\partial x_i} = -\frac{1}{\rho}\frac{\partial p}{\partial x_j} - \frac{\partial(\overline{u_i u_j})}{\partial x_i} \tag{2}$$

where ρ denotes the density of the fluid, u_i represents the time-averaged velocities, and p is the time-averaged pressure. Also, in this study, the results of numerical simulation for the culvert were compared against RNG k-ε turbulence model, standard k-ε and k-ω models. Results indicated that the RNG k-ε turbulence model predicts turbulent flow in the culvert with higher accuracy. Its results will be presented below.

3. Numerical simulation

In this study, Flow-3D software [46] was used to simulate the twin circular culvert. The Finite Volume Method (FVM) was employed to solve the three-dimensional governing equations. Fractional Area–Volume Obstacle Representation (FAVOR) method [47] was applied to detect the geometry of the structure. The FAVOR method uses the value of cell porosity and determines its value with a number between 0 and 1 separating solid boundaries from the fluid domain. The solver utilizes FVM and the VOF method to discretize and solve the governing equations and track the free surface of water. In the VOF method [45], a quantity is defined in each cell that indicates the ratio of water occupancy. A value of one indicates that the cell is completely filled with water and a value of zero indicates that the cell is empty. By knowing this quantity, the location of the water surface and its interfacial angle between the cells of the solution field is determined by the model. In addition, in simulating the twin circular culvert, no-slip conditions were applied at the contact surface of the fluid flow with the wall [48].

The Generalized Minimal Residual (GMRES) method has been used as an implicit pressure-velocity solver to establish pressure-velocity coupling. This method is very accurate and efficient for a wide range of problems and has excellent convergence, symmetry, and speed properties. However, it uses more memory than other methods. When the velocity, Reynolds stress, and continuity equation residuals reach values less than 10^{-6}, the convergent numerical solution is considered. Also, in all numerical models in this research, water density and dynamic viscosity and its temperature were set to 1000 kg/m^3, 0.001 N.s/m2 and 20°C, respectively.

The numerical simulation of the twin culvert is made according to the experimental model developed by Meselhe and Hebert [49]. The desired structure has the specifications presented in Fig.1. According to this figure, the length and diameter (D_o) of the culvert are 380 mm and 76 mm, respectively.

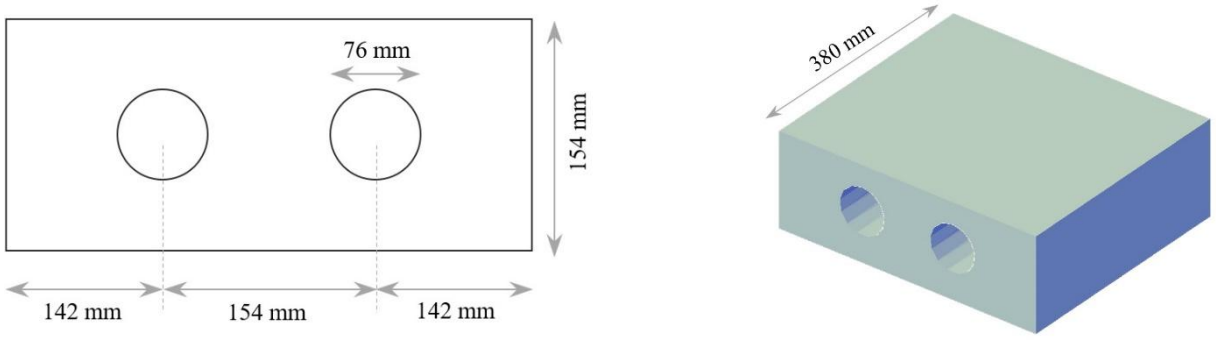

a) Section view **b) 3D view**

Fig. 1. Geometry of the twin circular culvert [29].

The laboratory experiments of Meselhe and Hebert [49] were performed at the University of Louisiana at Lafayette Hydraulic Engineering Laboratory. They were conducted in a flume consisting of a glass bed and walls supported by a stainless-steel frame. The flume is 0.438 m wide, 0.305 m deep, and 3.2 m long. In the laboratory tests, various conditions, including two parts, were examined. The first part includes a) flow passing through the culvert without allowing the flow to overtop (Culvert-only) b) closing

the culvert and passing the flow only over the culvert (Overtopping-only) c) flowing through the culvert and over the culvert with the gradual increase of the upstream water level (Combined-Rising) d) Flow passing through the culvert and on the culvert with the gradual decrease of the upstream water level (Combined-Receding). The second part includes a) unsteady hydrograph with rising and receding of upstream water level.

In the present numerical study, in the first part, only Combined-Receding and combined-Rising tests were simulated. Subsequently, the unsteady hydrograph of the inlet flow to the culvert was investigated. In the Combined-Receding simulation, the H/D_o increases from 1.3 to 3.3 (this means that the upstream water level changes from 0.1 m to 0.25 m), and in the Combined-Rising simulation, the H/D_o decreases from 3.3 to 1.3. These characteristics are presented in Fig. 2.

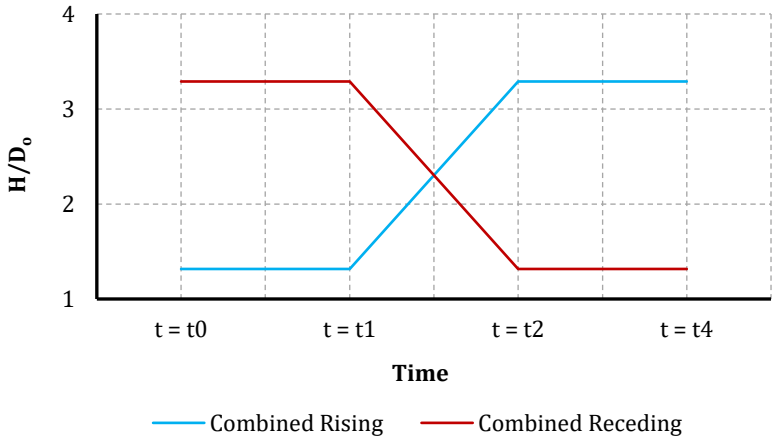

Fig. 2. Upstream water level change of the first part simulations.

The computational domain in the longitudinal direction is 100 cm from the upstream edge of the culvert and 40 cm from the downstream edge, with a width of 43.8 cm and a water depth of about 30 cm from the channel floor. For discretizing the computational domain, one mesh block was used (Fig. 3). The flow characteristic upstream of the culvert (x_{min}) was set to a certain depth and pressure. At the end of the domain, the flow will exit the computational domain (x_{max}) using the outlet boundary condition. The downstream boundary was defined as an outflow condition. This choice was justified by the fact that the flow at the outlet remained predominantly free-surface in all simulated scenarios, and no full submergence occurred. To prevent numerical instability and possible backflow effects, the computational domain was extended sufficiently downstream, and the velocity field near the outlet was monitored to ensure stable flow conditions. To simulate the water surface in contact with air (z_{max}), a symmetry condition was applied to simulate relative zero-pressure. All boundary conditions are presented in Table (1).

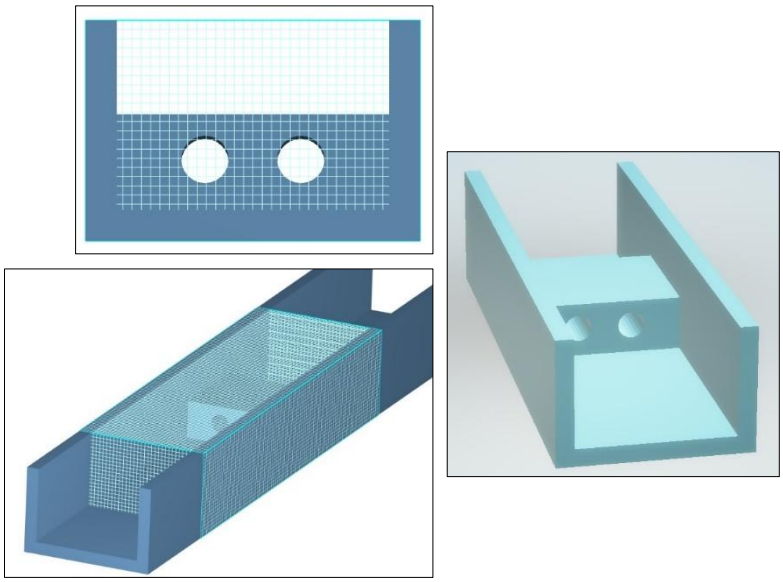

Fig. 3. Computational Grid.

Table 1. Boundary conditions in mesh blocks.

	Xmin	Xmax	Ymin	Ymax	Zmin	Zmax
Mesh Block	Specified Pressure	Outflow	Wall	Wall	Wall	Symmetry

The results are presented as dimensionless values according to standard design parameters [42]. The upstream water level (H) is normalized as H/D_o where D_o is the culvert diameter (0.076 m) and the dimensionless discharge Q^* is defined by $Q^* =$

$Q/\sqrt{g \times {D_o}^5}$.

3.1. Upstream water level rate sensitivity

As mentioned in the previous section and as shown in Fig. 2, to determine the hydraulic behavior of the culvert and how water drains downstream against variation in the upstream water level rate, H/D_o was increased from 1.3 to 3.3 (Rising-Models) and decreased from 3.3 to 1.3 (Receding-Models). The change in the upstream water level was implemented in the numerical model with different rates. For this purpose, to check the effect of this rate, H/D_o was changed from 3.3 to 1.3 and vice versa according to Table (2), and the effect of each of these conditions on the head-discharge curve was evaluated.

Table 2. Model characteristics to investigate the effect of upstream water level variation rate.

Receding Models					Rising Models				
Name	**t (s)**	**H (m)**	**H/Do**	**Rate (head (m)/s)**	**Name**	**t (s)**	**H (m)**	**H/Do**	**Rate (head (m)/s)**
	0	0.25	3.3			0	0.1	1.3	
CRE-1	30	0.25	3.3	-0.0100	**CRI-1**	30	0.1	1.3	0.0100
	45	0.1	1.3			45	0.25	3.3	
	0	0.25	3.3			0	0.1	1.3	
CRE-2	30	0.25	3.3	-0.0050	**CRI-2**	30	0.1	1.3	0.0050
	60	0.1	1.3			60	0.25	3.3	
	0	0.25	3.3			0	0.1	1.3	
CRE-3	30	0.25	3.3	-0.0033	**CRI-3**	30	0.1	1.3	0.0033
	75	0.1	1.3			75	0.25	3.3	
	0	0.25	3.3			0	0.1	1.3	
CRE-4	30	0.25	3.3	-0.0025	**CRI-4**	30	0.1	1.3	0.0025
	90	0.1	1.3			90	0.25	3.3	
	0	0.25	3.3			0	0.1	1.3	
CRE-5	30	0.25	3.3	-0.0020	**CRI-5**	30	0.1	1.3	0.0020
	105	0.1	1.3			105	0.25	3.3	

Fig. 4 shows the curves head-discharge changes for the receding and rising models. As seen in Fig. 4. a, CRE-2 to CRE-5 models exhibit consistency, but CRE-1 deviates from the others. Thus, receding models with rates slower than -0.0050 m/s (CRE-2 onward) show negligible rate dependency. Similarly, in Fig. 4. b, models CRI-2 to CRI-5 match each other, while CRI-1 diverges from the others. Therefore, rising models with rates below 0.0050 m/s (CRI-2 onward) are appropriate.

The deviation observed in the fastest rate cases (CRE-1 and CRI-1) can be attributed to physical flow behavior rather than numerical instability. At high rates of upstream water level variation, the flow does not have sufficient time to fully develop and adjust to changing boundary conditions. This results in a transient lag between head and discharge, reflecting the hysteretic nature of unsteady flow. Therefore, these deviations represent a real hydraulic phenomenon associated with flow inertia and turbulence effects.

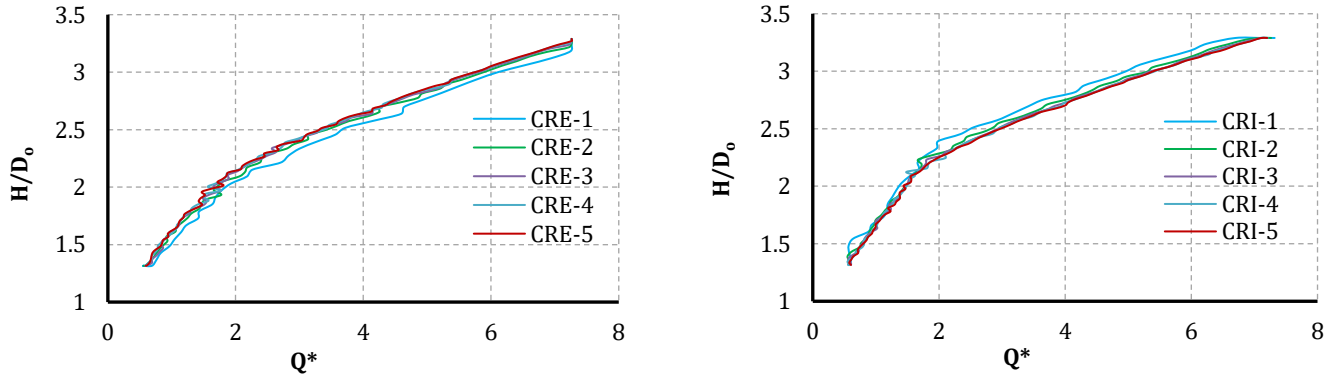

a) Receding models **b) Rising models**

Fig. 4. Head-discharge curves for different water level variation rate.

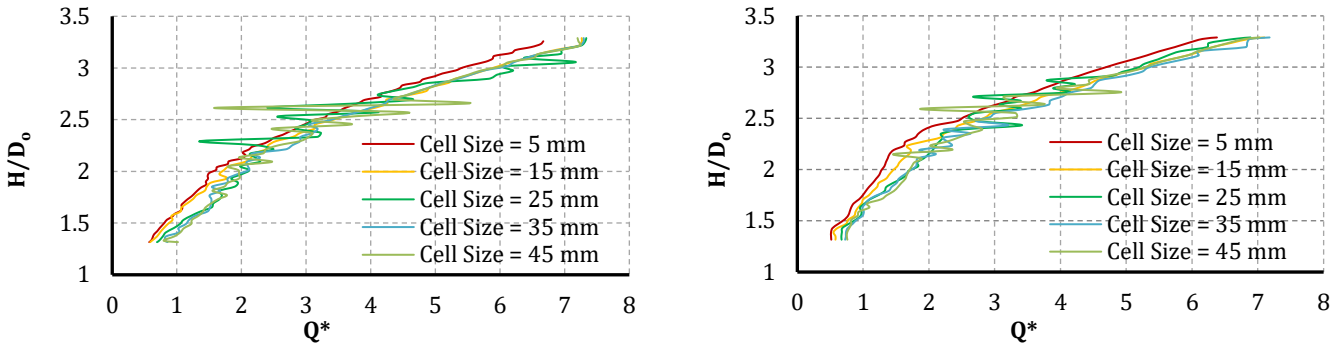

a) Receding models CRE-2 b) Rising models CRI-2

Fig. 5. Head-discharge curves for different cell sizes.

3.2. Mesh cell size sensitivity

To study the independence of the research results from the mesh cell size, both receding and rising models, including CRE-2 and CRI-2 models, with five different cell sizes in the range of 5 to 45 mm were simulated. In all cases, the head-discharge curve was considered as a criterion for selecting the optimal cell size. The effect of cell size on these curves' accuracy is shown in Fig. 5. The results show that the head-discharge curve for cell sizes of 25, 35, and 45 mm differs from the other two meshes in both receding and rising models, but there is a slight difference between the predicted head-discharge curve of cell sizes of 5 and 15 mm. Therefore, to reduce the simulation time, a 15 mm cell size is selected as the optimal mesh cell size.

3.3. Turbulence model study

To use a suitable turbulence model for predicting the turbulent flow in the culvert, the effect of applying different turbulence models, including RNG, *k-ε* and *k-ω* on the head-discharge curve was evaluated. For this purpose, the CRE-2 receding model and CRI-2 rising model with a cell size of 15 mm were simulated with three different turbulence models. In Fig. 6, the head-discharge curve for different turbulence models for receding and rising models is compared with the experimental results of Meselhe and Hebert [49]. The results show that all three turbulence models can predict the turbulent flow inside the culvert with high accuracy. Therefore, the RNG model was selected for the following models.

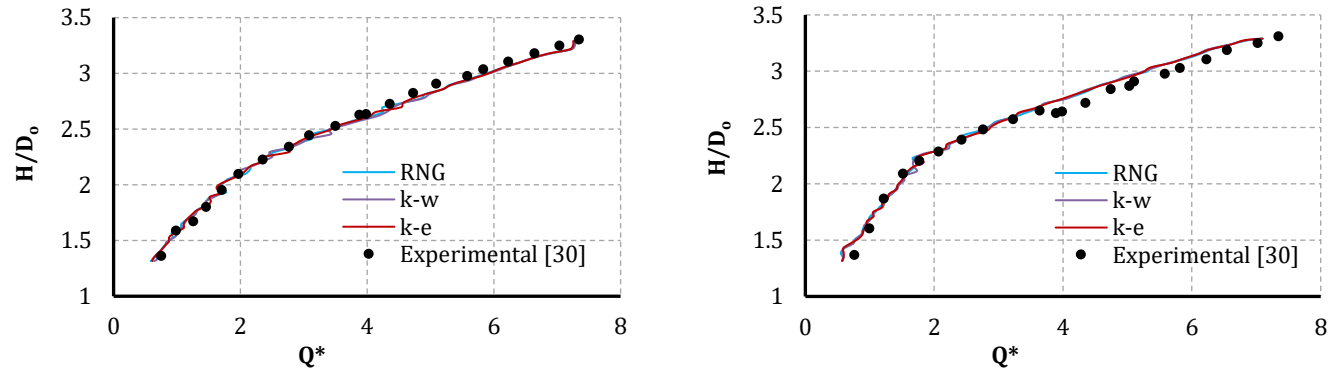

a) Receding model of CRE-2 b) Rising model of CRI-2

Fig. 6. Head-discharge curves for different turbulence models.

3.4. Numerical model validation

To validate the numerical model, the results of the present study are compared with the results of Meselhe and Hebert [49] experimental results. Fig. 6 compares the head-discharge curve in the present numerical model (RNG turbulence model) and Meselhe and Hebert [49] laboratory results, for receding and rising models, respectively. The results of these two figures show that the numerical model accurately predicts the head-discharge curve compared to the laboratory curve with excellent agreement. The percent error is 1.3% for the receding model and 2.3% for the rising model.

4. Results and discussion

In this section, the details of the head-discharge characteristics in the twin circular culvert will be investigated.

4.1. Combined receding and rising

Fig. 7 illustrates the flow field for the rising condition with $H/D_o = 3.3$. Qualitative analysis of the flow reveals that the maximum velocity occurs at the point where the flow impacts the downstream bed. Additionally, the flow passing over the culvert exhibits higher velocity at its intersection with the flow passing through the culvert, likely due to the greater free fall of the overtopping flow. Furthermore, the flow field observation indicates three rotational flow regions with negligible velocity, trapped in place. These three regions are located along the lateral sides, in the middle of the channel, and adjacent to the downstream side

of the culvert.

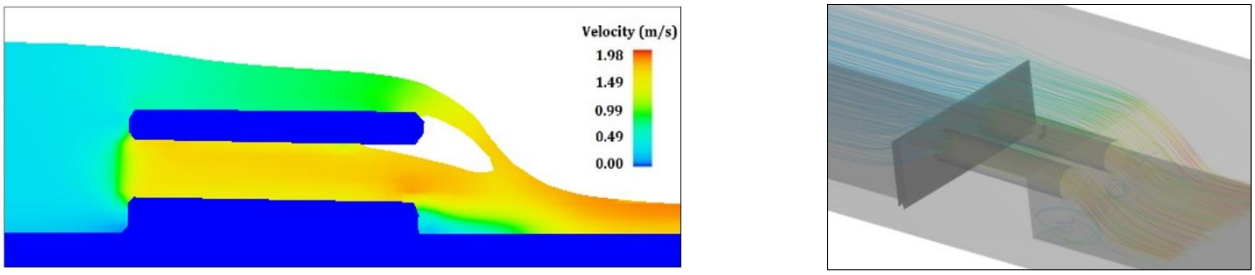

a) Longitudinal cross-section through the center of the culvert **b) Three-dimensional streamlines**

Fig. 7. Velocity field of the flow simultaneously passing through and over the culvert ($H/D_o = 3.3$).

Fig. 8. a shows the discharge passing through the culvert and over the culvert (culvert overtopping) during the rising of H/D_o from 1.3 to 3.3. As can be seen, when H/D_obetween 1.3 to about 2.3 ranges, the overtopping discharge is zero. The parameter of discharge per head ($Q^*/\left(\frac{H}{D_o}\right)$) passing through the culvert during the rising of H/D_o from 1.3 to 3.3 remains nearly constant at 1.573. Also, this parameter ($Q^*/\left(\frac{H}{D_o}\right)$) for discharge passing over the culvert is much higher than the discharge passing through the culvert. When H/D_o is higher than 2.3, this parameter is almost equal to 3.877. This is due to the free flow passing over the culvert and the greater width of the flow than through the culvert. Also, Fig. 8. b shows the percentage of discharge passing through the culvert structure and the flow passing over the culvert for different H/D_o for rising models. It can only be seen that near the $H/D_o =$ 2.3, the Q^* shows a slight fluctuation.

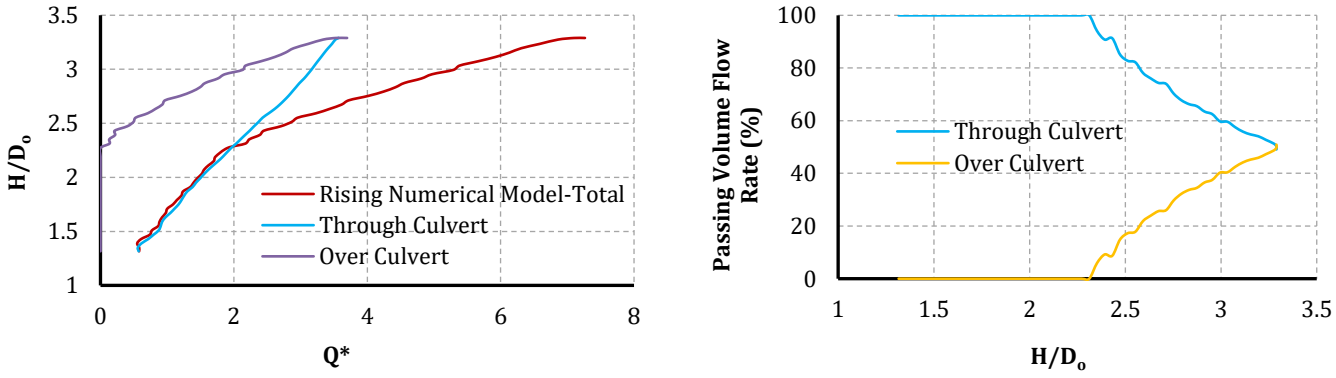

a) Head-Discharge **b) Discharge Percent**

Fig. 8. Discharge passing through and over the culvert in rising model.

Fig shows discharge passing through the culvert and over the culvert during the receding of H/D_o from 3.3 to 1.3. As can be seen, when H/D_o ranges from 1.3 to ~2, the discharge over the culvert is zero. The parameter of discharge per head ($Q^*/\left(\frac{H}{D_o}\right)$) passing through the culvert during the receding of H/D_o from 3.3 to 1.3 is almost constant and equals 1.639. Also, this parameter ($Q^*/\left(\frac{H}{D_o}\right)$) for discharge passing over the culvert is much higher than the discharge passing through the culvert. when H/D_o is higher than 2, this parameter is almost equal to 3.175. This is due to the free flow passing over the culvert and the greater width of the flow than through the culvert.

The results show that the discharge rate ($Q^*/\left(\frac{H}{D_o}\right)$) from inside the culvert in receding models (1.639) is higher than in rising models (1.639), while the discharge rate over the culvert in rising models (3.877) is higher than in receding models (3.175).

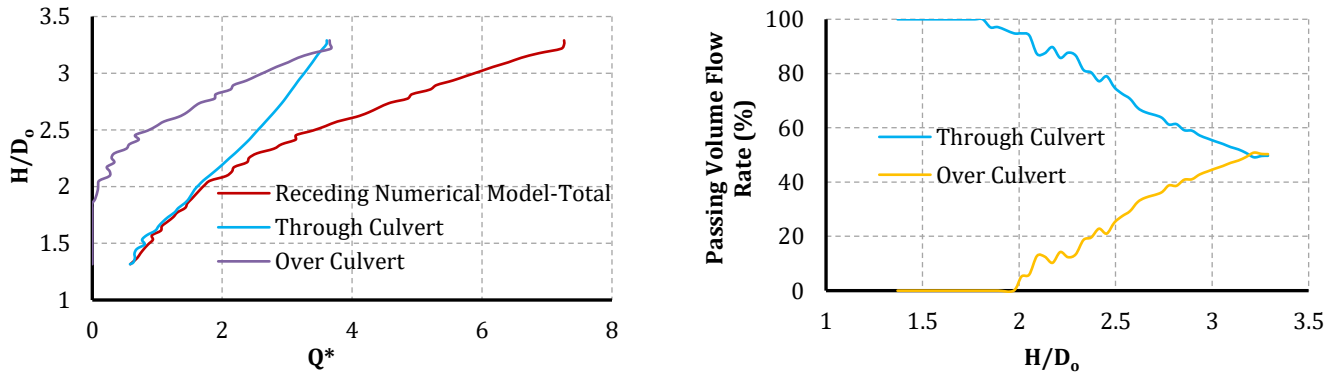

a) Head-Discharge **b) Discharge Percents**

Fig. 9. Discharge passing through and over the culvert in receding model.

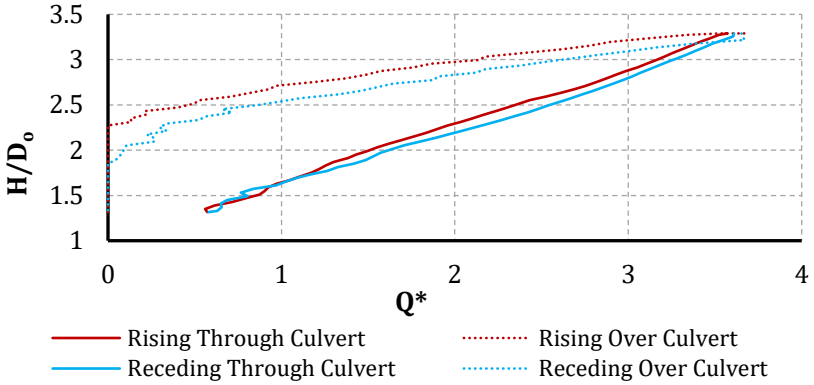

Fig. 10. Discharge passing through and over the culvert in receding and rising models.

In Fig. 10, the discharge changes over the culvert and through the culvert are shown simultaneously for the rising and receding models. It can be seen that the discharge passing through the culvert for the two models of rising and receding shows no significant difference, but the discharge passing over the culvert in the two mentioned models is completely different, and for the same heads, the receding model has a higher discharge.

4.2. Unsteady hydrograph

In this section, the effect of the unsteady flow on the hydraulic performance of the twin culvert was investigated. The upstream water level has both rising and receding limbs as shown in Fig. 10 (Upstream Head-Time curve). In the numerical model, the upstream water level was used to investigate discharge downstream of the culvert, as well as over and through the culvert.

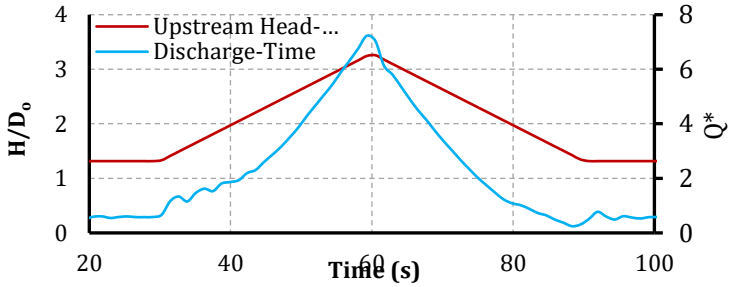

Fig. 11. Head-discharge curves for unsteady hydrograph including rising and receding limbs.

Fig. 11 shows the head-discharge curve versus time for the hydrograph. According to the figure, the rising limb of the discharge curve has a lower slope than the receding limb, and the discharge has reached the minimum in a shorter period of time. In the rising limb, it can be seen that from about time equal to 35 s, non-dimensional volume flow rate Q^* has reached 1.47 to 7 in about time equal to 60 s, showing the Q^* increasing in the rising limb is equal to 0.22, while, in the receding limb, it can be seen that from about time equal to 60 s, the Q^* has reached 7 to 1.48 in about time equal to 77 s, that show the approximate rate of outlet flow decreasing in the receding limb is equal to 0.32. The results indicate that, under the specific conditions of the present study, the discharge during the receding limb is approximately 1.5 times higher than during the rising limb. It should be noted that this ratio is dependent on the culvert geometry and hydrograph characteristics and may vary under different conditions. However, the general trend of higher discharge during the receding phase reflects the hysteretic behavior of unsteady flow in culverts.

In Fig. 12, the discharge passing percentage over the culvert and through the culvert is given for the unsteady hydrograph. For this purpose, this curve is presented in two separate sections for the rising limb and the receding limb. According to the figure, it can be seen that in the rising limb at depths close to the surface of the culvert, the passing percentages fluctuate greatly, while in the receding limb at $H/D_o < 2.4$, the discharge completely passes through the culvert.

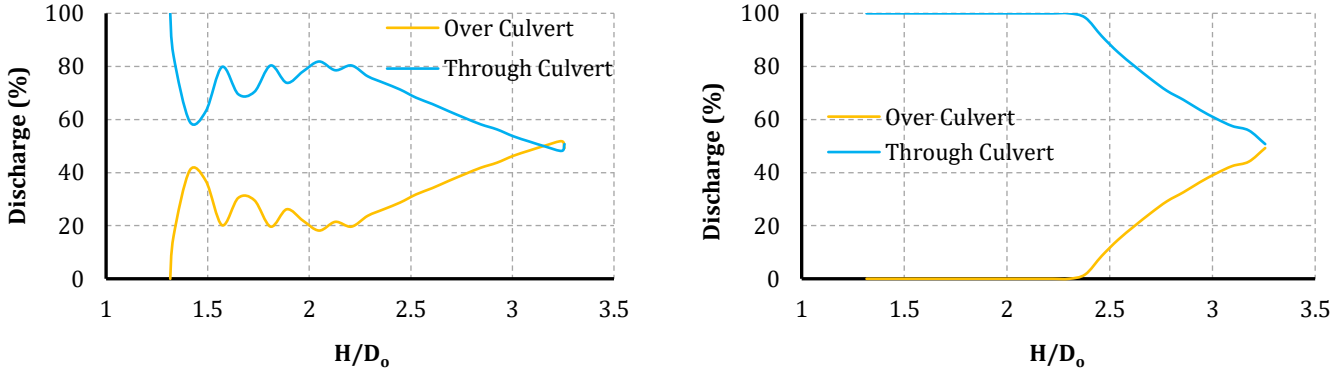

Fig. 12. Passing discharge percent for unsteady hydrograph.

4.3. Data-driven modeling and machine learning analysis

In addition to the numerical simulations, a series of data-driven modeling techniques were applied to predict the discharge behavior of the twin circular culvert under various hydraulic conditions. The purpose of this complementary analysis was to evaluate the ability of machine learning algorithms to reproduce the complex, nonlinear relationship between the upstream water depth and the corresponding discharge, as presented in both numerical and laboratory data. The use of multiple machine learning algorithms was intended not only to evaluate predictive performance but also to compare different modeling approaches in capturing nonlinear hydraulic behavior. This comparative analysis helps identify the most reliable and robust model for practical applications. The dataset used for training and validation included upstream head values as input features and the measured or simulated discharge values as output targets. The models were trained and evaluated separately for rising and receding water levels to account for the hysteretic behavior of culvert flow. A total of eight algorithms with distinct learning paradigms were implemented using the Orange data mining platform, including Random Forest (RF), K-Nearest Neighbors (KNN), Decision Tree (Tree), Gradient Boosting (GB), Support Vector Machine (SVM), Linear Regression (LR), AdaBoost (AB), and Neural Network (NN). The choice of these algorithms was motivated by their ability to represent both linear and nonlinear mappings. Ensemble methods such as Random Forest, Gradient Boosting, and AdaBoost were included because of their high accuracy and robustness in regression problems, while the Neural Network model was incorporated to evaluate the potential of deep learning for capturing higher-order nonlinearities in the flow regime. Model performance was assessed using standard statistical indicators—mean squared error (MSE), root mean square error (RMSE), mean absolute error (MAE), mean absolute percentage error (MAPE), and coefficient of determination (R^2), to ensure consistent comparison.

The dataset consisted of 51 data points obtained from numerical simulations and 22 data points obtained from experimental measurements. The input parameter included the normalized upstream head (H/D_o), while the output variable was the dimensionless discharge. The data were divided into training and testing sets using an 80-20 split. In addition, k-fold cross-validation was applied to ensure robustness and avoid overfitting.

The results of the numerical dataset showed a clear dominance of ensemble-based algorithms. For the rising head condition, Gradient Boosting and AdaBoost achieved the best performance, with R^2 values of approximately 0.992 and RMSE around 0.176, indicating excellent agreement with the simulated discharges. KNN and Random Forest also exhibited strong performance ($R^2 > 0.988$), confirming their ability to generalize the underlying nonlinear trends. In contrast, Linear Regression yielded the lowest accuracy ($R^2 = 0.914$), reflecting the inadequacy of a linear model in representing the hydraulic relationship between head and discharge. During the receding phase, KNN, Gradient Boosting, and AdaBoost maintained superior predictive capability ($R^2 \approx 0.992$, RMSE ≈ 0.18), while the Random Forest model remained competitive with slightly higher error values. The overall numerical results confirmed that ensemble learning and local-instance-based methods can effectively capture the nonlinearities inherent in the CFD-based head–discharge relationship.

The results obtained from the experimental dataset followed a similar trend but with slightly larger errors due to unavoidable measurement uncertainties and physical variability. For the rising condition, the Neural Network achieved the best performance ($R^2 = 0.980$, RMSE = 0.284), demonstrating its capability to adapt to experimental noise while maintaining high predictive accuracy. Gradient Boosting and AdaBoost ranked second and third ($R^2 \approx 0.948$), proving again the reliability of boosting-based ensembles in hydraulic prediction. The weakest model was the single Decision Tree ($R^2 = 0.848$), which tends to overfit limited data. For the receding experimental dataset, the Neural Network once more outperformed all other algorithms ($R^2 = 0.985$, RMSE = 0.249), followed closely by Gradient Boosting and AdaBoost ($R^2 \approx 0.969$). These outcomes highlight that data-driven approaches, particularly those with adaptive or ensemble learning mechanisms, can successfully approximate the nonlinear discharge behavior even in laboratory environments.

Comparing the performance between rising and receding conditions reveals that the models generally achieved higher accuracy in the receding phase. This can be attributed to the more stable hydraulic regime during flow recession, where turbulence intensity and free-surface fluctuations are less pronounced. Consequently, the receding limb provides smoother relationships between head and discharge, allowing machine learning models to fit the data more consistently. This behavior mirrors the hysteretic characteristics identified in the CFD simulations, where discharge during the receding limb was higher for the same head values compared to the rising limb. The close agreement between these two modeling approaches demonstrates that machine learning can not only complement but also validate numerical simulation outcomes. The difference in model performance between numerical and experimental datasets can be explained by the intrinsic characteristics of the data and the learning mechanisms of the algorithms. The experimental dataset contains measurement uncertainties and noise, which makes flexible models such as Neural Networks more suitable due to their ability to capture complex nonlinear patterns and generalize under noisy conditions. In contrast, the numerical dataset is smoother and more structured, allowing ensemble methods such as Gradient Boosting to achieve higher accuracy by effectively learning precise relationships without being affected by noise. This highlights the importance of selecting machine learning models based on data characteristics. This behavior also suggests that Neural Networks can implicitly act as noise-tolerant models, effectively reducing the influence of experimental uncertainties during the learning process.

The quantitative comparison of models' performance for each condition is presented in Tables 3 and 4. The statistical performance metrics presented in Tables 3 and 4 correspond to the testing dataset.

Table 3. Statistical evaluation metrics for the numerical simulations.

	Rising					Receding				
Model	**MSE**	**RMSE**	**MAE**	**MAPE**	**R^2**	**MSE**	**RMSE**	**MAE**	**MAPE**	**R^2**
Random Forest	0.044	0.210	0.144	6.061	0.988	0.105	0.324	0.262	9.540	0.976
kNN	0.043	0.208	0.128	5.410	0.989	0.059	0.243	0.136	7.048	0.987
Tree	0.100	0.316	0.236	9.305	0.974	0.048	0.218	0.162	6.860	0.989
Gradient Boosting	0.031	0.176	0.134	4.877	0.992	0.075	0.274	0.209	7.738	0.983
SVM	0.069	0.262	0.134	6.598	0.982	0.224	0.474	0.400	23.794	0.949
Linear Regression	0.329	0.573	0.483	31.233	0.914	0.033	0.182	0.125	5.070	0.992
AdaBoost	0.031	0.176	0.132	4.724	0.992	0.034	0.185	0.157	6.003	0.992
Neural Network	0.121	0.348	0.265	11.370	0.968	0.034	0.183	0.154	5.832	0.992

Table 4. Statistical evaluation metrics for the experimental simulations.

	Rising					Receding				
Model	**MSE**	**RMSE**	**MAE**	**MAPE**	**R^2**	**MSE**	**RMSE**	**MAE**	**MAPE**	**R^2**
Random Forest	0.379	0.615	0.538	22.518	0.904	0.268	0.518	0.356	16.477	0.936
kNN	0.370	0.609	0.438	19.439	0.907	0.229	0.479	0.318	12.732	0.945
Tree	0.603	0.777	0.687	24.221	0.848	0.417	0.646	0.516	16.087	0.900
Gradient Boosting	0.204	0.451	0.407	13.870	0.949	0.128	0.358	0.334	11.970	0.969
SVM	0.439	0.662	0.384	18.957	0.889	0.325	0.570	0.307	14.185	0.922
Linear Regression	0.509	0.714	0.537	30.052	0.872	0.248	0.498	0.412	19.420	0.941
AdaBoost	0.207	0.455	0.411	13.931	0.948	0.128	0.358	0.334	11.969	0.969
Neural Network	0.081	0.284	0.242	8.484	0.980	0.062	0.249	0.173	4.851	0.985

Table 3 lists the statistical evaluation metrics for the rising and receding datasets obtained from the numerical simulations, while Table 4 provides the corresponding results derived from the laboratory experiments. In both tables, the ensemble-based and neural network models consistently outperform traditional algorithms, confirming their ability to represent the strongly nonlinear hydraulic processes involved in culvert flow.

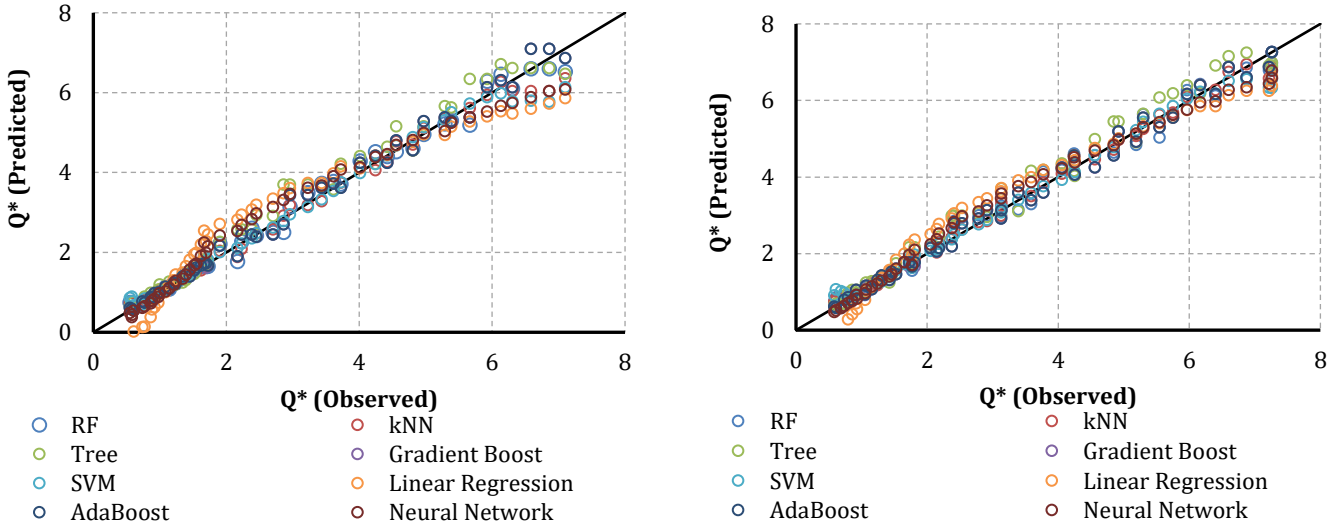

a) Rising model **b) Receding model**

Fig. 13. Comparison between observed and predicted discharge values for numerical datasets using different machine learning models.

Fig. 13 presents a comparison between the observed laboratory discharges and those predicted by various machine learning models. The Neural Network and ensemble models (Gradient Boosting and AdaBoost) show the best alignment with the 1:1 line, confirming their capability to generalize experimental flow behavior under both rising and receding conditions.

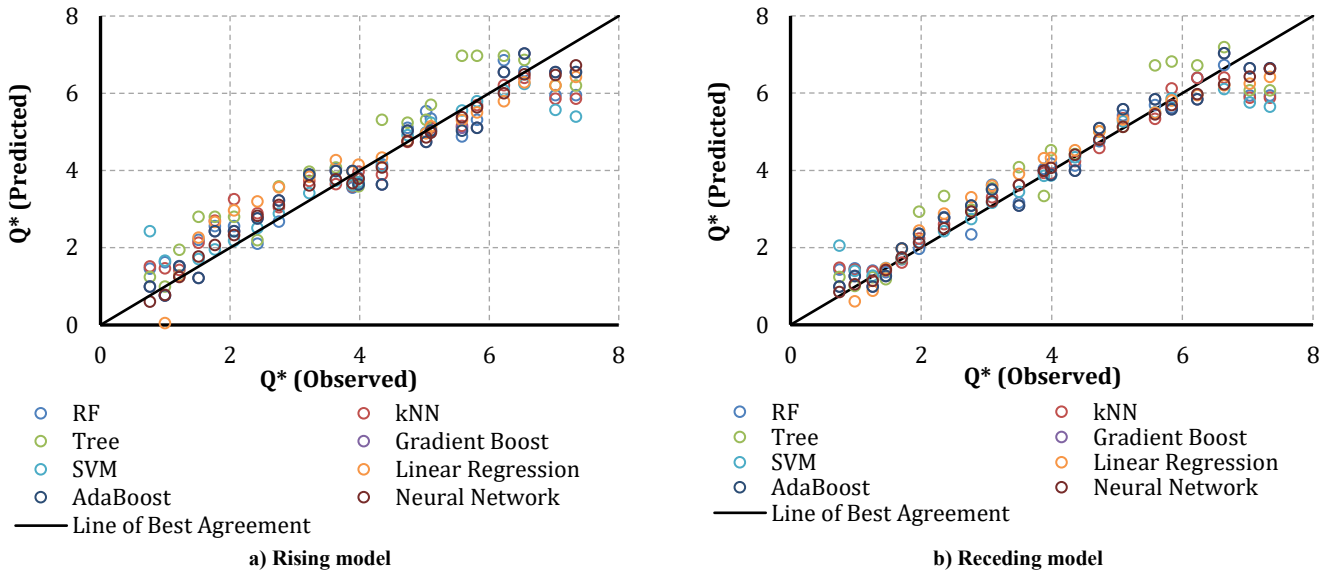

Fig. 14. Comparison between observed and predicted discharge values for experimental datasets using different machine learning models.

Fig. 14 illustrates the relationship between the observed (Flow-3D simulated) and predicted discharge values for both rising and receding conditions. The close clustering of points around the 1:1 reference line indicates that ensemble and neighborhood-based models (particularly Gradient Boosting, AdaBoost, and KNN) provide the highest accuracy in reproducing the numerical discharge behavior of twin circular culverts.

Overall, the data-driven modeling results demonstrate that machine-learning approaches can effectively complement physics-based CFD simulations. The strong consistency between the numerical, experimental, and ML-based predictions supports the feasibility of hybrid modeling frameworks in hydraulic engineering. Such frameworks can significantly reduce computational time while maintaining high accuracy, offering a reliable tool for discharge estimation and culvert design optimization under varying flow conditions. The performance of the machine learning models in this study is consistent with previous research in hydraulic engineering, where ensemble methods and neural networks have shown superior capability in capturing nonlinear flow behavior. Compared to earlier studies, the achieved accuracy (R^2 up to 0.99) indicates a high level of reliability in predicting culvert discharge under unsteady flow conditions.

5. Summary and conclusion

This research comprehensively analyzed the hydraulic behavior of twin circular culverts under unsteady flow conditions using numerical simulations complemented by data-driven modeling. The study examined the effects of rising and receding inlet flows, upstream water level variations, and unsteady hydrographs on culvert discharge and flow distribution. Numerical modeling was performed by solving the Reynolds-Averaged Navier–Stokes (RANS) equations for incompressible flow with the RNG k–ε turbulence model, providing reliable predictions of turbulent flow fields and discharge characteristics. Validation against laboratory data confirmed excellent agreement, ensuring that the chosen turbulence model and computational setup accurately captured the observed physical flow features. Sensitivity analyses on mesh resolution, turbulence modeling, and upstream water level variation rates further ensured the robustness and convergence of the numerical results.

The numerical simulations revealed that through-flow discharge during the rising phase (H/Do = 1.3–3.3) remained nearly constant at approximately 1.573 $m^3/s/m$, while overtopping discharge increased substantially after the upstream head exceeded 2.3, reaching nearly 3.877 $m^3/s/m$. In the receding phase, through-flow discharge stayed roughly constant at 1.639 $m^3/s/m$, whereas overtopping discharge reached around 3.175 $m^3/s/m$ before the head ratio fell below 2. Overall, through-flow discharge differed only slightly between rising and receding stages (≈4%), but overtopping discharge showed a significant difference of ≈22%. The rising limb of the unsteady hydrograph exhibited a lower slope than the receding limb, indicating that outflow during recession was about 1.5 times higher. At shallow depths near the culvert crown, flow distribution fluctuated considerably during the rising limb, while for H/Do < 2.4 in the receding limb, nearly all discharge passed through the culvert.

To complement the numerical results, a data-driven modeling framework using machine learning algorithms was developed to evaluate whether AI methods could replicate the nonlinear hydraulic behavior observed in CFD and laboratory data. Eight algorithms were tested using the Orange data mining platform, including Random Forest (RF), K-Nearest Neighbors (KNN), Decision Tree, Gradient Boosting (GB), Support Vector Machine (SVM), Linear Regression (LR), AdaBoost (AB), and Neural Network (NN). Model performance was evaluated separately for rising and receding phases using R^2, RMSE, MAE, and MAPE metrics. The results indicated that ensemble-based models and neural networks effectively captured the complex discharge–head relationships. For numerical data, Gradient Boosting and AdaBoost achieved the highest accuracy ($R^2 \approx 0.992$, RMSE ≈ 0.176), followed by KNN and Random Forest, while Linear Regression performed weakest, confirming the strong nonlinearity of the system. For experimental data, the Neural Network achieved the best accuracy ($R^2 = 0.980$ for rising, $R^2 = 0.985$ for receding), closely followed by Gradient Boosting and AdaBoost. In both datasets, models performed better during the receding phase, likely

due to more stable flow conditions.

The integration of numerical and data-driven approaches provides complementary insights into culvert hydraulics: CFD models offer detailed flow visualization and physical interpretation, while machine learning enables rapid discharge prediction with low computational cost once trained. The strong agreement among experimental, numerical, and AI-based results confirms that hybrid modeling can enhance predictive accuracy, improve design efficiency, and serve as a reliable tool for assessing flow transitions, discharge hysteresis, and unsteady hydraulic responses in culverts and similar drainage structures.

Statements & Declarations

Author contributions

Ehsan Behnamtalab: Conceptualization, Investigation, Methodology, Writing - Review & Editing.

Mohsen Behnamtalab: Formal analysis, Validation, Writing - Original Draft, Writing - Review & Editing.

Funding

The authors received no financial support for the research, authorship, and/or publication of this article.

Data availability

The data presented in this study will be available on request from the corresponding author.

Declarations

The authors declare no conflict of interest.

References

[1] Norman, J. M., Houghtalen, R.J. and Johnston, W.J Hydraulic design of highway culverts. Second ed. Washington, DC (US): FHWA; 2001.

[2] Chang, H.-K., Tan, Y.-C., Lai, J.-S., Pan, T.-Y., Liu, T.-M., Tung, C.-P. Improvement of a drainage system for flood management with assessment of the potential effects of climate change. Hydrological Sciences Journal, 2013; 58: 1581–1597. doi:10.1080/02626667.2013.836276.

[3] Mamo, T. G. Evaluation of the Potential Impact of Rainfall Intensity Variation due to Climate Change on Existing Drainage Infrastructure. Journal of Irrigation and Drainage Engineering, 2015; 141: 05015002. doi:10.1061/(ASCE)IR.1943-4774.0000887.

[4] Pereira, M., Fernandes, L., Macário, E., Gaspar, S., Pinto, J. Climate Change Impacts in the Design of Drainage Systems: Case Study of Portugal. Journal of Irrigation and Drainage Engineering, 2015; 141: 05014009. doi:10.1061/(ASCE)IR.1943-4774.0000788.

[5] Todeschini, S. Trends in long daily rainfall series of Lombardia (northern Italy) affecting urban stormwater control. International Journal of Climatology, 2012; 32: 900–919. doi:10.1002/joc.2313.

[6] Wang, S., Feng, Z., Guo, C., Wei, J., Zhao, R. Research on the method of identifying vertical earth pressure of hinged prefabricated culvert box culvert on the top slab. Scientific Reports, 2024; 14: 18844. doi:10.1038/s41598-024-69893-4.

[7] Gao, C., Elzarka, H. The use of decision tree based predictive models for improving the culvert inspection process. Advanced Engineering Informatics, 2021; 47: 101203. doi:10.1016/j.aei.2020.101203.

[8] Othman, K., Kavianpour, M., Amini, A., Aminpour, Y. A state-of-the-art review of physical modeling of scouring at the culvert outlet. ISH Journal of Hydraulic Engineering, 2024; 30: 1–8. doi:10.1080/09715010.2024.2340626.

[9] Ahmed, K. O., Kavianpour, M. R., Amini, A., Aminpour, Y. Physical modeling of the effect of shape, blockage, and flow variability on scour in culvert outlets. PLoS One, 2024; 19: e0306252. doi:10.1371/journal.pone.0306252.

[10] Dasika, B. New Approach to Design of Culverts. Journal of Irrigation and Drainage Engineering, 1995; 121: 261–264. doi:10.1061/(ASCE)0733-9437(1995)121:3(261).

[11] Montes, J. S., Dasika, B. Discussion and Closure: New Approach to Design of Culverts. Journal of Irrigation and Drainage Engineering, 1997; 123: 71–72. doi:10.1061/(ASCE)0733-9437(1997)123:1(71).

[12] Hager, W. H., Giudice, G. D. Generalized Culvert Design Diagram. Journal of Irrigation and Drainage Engineering, 1998; 124: 271–274. doi:10.1061/(ASCE)0733-9437(1998)124:5(271).

[13] Johnson, P., Brown, E. Stream Assessment for Multicell Culvert Use. Journal of Hydraulic Engineering-asce - J HYDRAUL ENG-ASCE, 2000; 126: 381–386. doi:10.1061/(ASCE)0733-9429(2000)126:5(381).

[14] Ansar, M., Alexis, A., Damisse, E. Flow computations at Kissimmee River gated structures: A comparative study. South Florida (FL): Hydrology and Hydraulics Dept; 2002. Report No.:

[15] Lee, K. S., Jin, R. S. Development of program for box culverts design. In: Proceedings of the 35th Conference; 2003; South Korea. p. 2686–2689.

[16] Ku, H. J., Jun, K. S. Development of culvert design model. In: Proceedings of Korea Water Resources Association Conference; 2008; South Korea. p. 645–649.

[17] Richmond, M. C., Deng, Z., Guensch, G. R., Tritico, H., Pearson, W. H. Mean flow and turbulence characteristics of a full-scale spiral corrugated culvert with implications for fish passage. Ecological Engineering, 2007; 30: 333–340. doi:10.1016/j.ecoleng.2007.04.011.

[18] Chanson, H. Hydraulics of open channel flow. Second ed. London (UK): Elsevier; 2004. doi:10.1016/B978-0-7506-5978-9.X5000-4.

[19] Chow, V. T. Open-Channel Hydraulic. First ed. Columbus (OH): McGraw-Hill Education; 1959.

[20] Yoo, D.-H., Lee, S. Direct determination of the width or the height for a box culvert applying dimensionless equations. KSCE Journal of Civil Engineering, 2012; 16: 1302–1307. doi:10.1007/s12205-012-1695-1.

[21] Kang, M. S., Koo, J. H., Chun, J. A., Her, Y. G., Park, S. W., Yoo, K. Design of drainage culverts considering critical storm duration. Biosystems Engineering, 2009; 104: 425–434. doi:10.1016/j.biosystemseng.2009.07.004.

[22] May, L. W. Hydraulic Design Handbook. First ed. Columbus (OH): McGraw-Hill Education; 1999.

[23] Schall, J. D., Thompson, P. L., Zerges, S. M., Kilgore, R. T., Morris, J. L. Hydraulic Design of Highway Culverts. Third ed. Washington, DC (US): FHWA; 2012.

[24] French, J. L. First Progress Report on Hydraulics of Short Pipes: Hydraulic Characteristics of Commonly Used Pipe Entrances. Washington, DC (US): U.S. Dept. of Commerce, National Bureau of Standards; 1955. Report No.: NBS Report no. 4444.

[25] French, J. L. Second Progress Report on Hydraulics of Culverts: Pressure and Resistance Characteristics of a Model Pipe Culvert. Washington, DC (US): U.S. Dept. of Commerce, National Bureau of Standards; 1956. Report No.: NBS Report no. 4911.

[26] French, J. L. Third Progress Report on Hydraulics of Culverts: Effect of Approach Channel Characteristics on Model Pipe Culvert Operation. Washington, DC (US): U.S. Dept. of Commerce, National Bureau of Standards; 1957. Report No.:

[27] French, J. L. Fourth Progress Report on Hydraulics of Culverts: Hydraulics of improved Inlet Structures for Pipe Culverts. Washington, DC (US): U.S. Dept. of Commerce, National Bureau of Standards; 1961. Report No.: NBS Report no. 7178.

[28] French, J. L. Sixth progress report on hydraulics of culverts: Tapered box culvert inlets. Washington, DC (US): U.S. Dept. of Commerce, National Bureau of Standards; 1966. Report No.: NBS Report no. 9355.

[29] French, J. L., Bossy, H. G. Seventh progress report on hydraulics of culverts: Tapered box culvert inlets with fall concentration in the inlet structure. Washington, DC (US): U.S. Dept. of Commerce, National Bureau of Standards; 1967. Report No.: NBS Report no. 9528.

[30] Lyn, D., Dey, S., Saksena, S., Merwade, V. Culvert versus Bridge Hydraulics for Larger-Span or Short Culverts. Journal of Hydraulic Engineering, 2024; 150: 04024002. doi:10.1061/JHEND8.HYENG-13650.

[31] Bodhaine, G. L. Measurement of peak discharge at culverts by indirect methods. Washington, DC (US): US Government Printing Office; 1968. Report No.: 03-A3.

[32] Aly, A. M. Machine Learning Reshaping Computational Fluid Dynamics: A Paradigm Shift in Accuracy and Speed. Fluids, 2025; 10: 275. doi:10.3390/fluids10100275.

[33] Mao, R., Lan, Y., Liang, L., Yu, T., Mu, M., Leng, W., Long, Z. Rapid CFD Prediction Based on Machine Learning Surrogate Model in Built Environment: A Review. Fluids, 2025; 10: 193. doi:10.3390/fluids10080193.

[34] Nie, Y., Yu, K. H., Wang, Y., Liu, P. Applications of machine learning and deep learning in hydrology from a bibliometric perspective: a comprehensive review. Discover Artificial Intelligence, 2025; 5: 242. doi:10.1007/s44163-025-00471-x.

[35] Jafari, S. M., Zahiri, A. R., Bozorg Hadad, O., Mohammad Rezapour Tabari, M. A hybrid of six soft models based on ANFIS for pipe failure rate forecasting and uncertainty analysis: a case study of Gorgan city water distribution network. Soft Computing, 2021; 25: 7459–7478. doi:10.1007/s00500-021-05706-4.

[36] Tabari, M. M. R., Sanayei, H. R. Z. Prediction of the intermediate block displacement of the dam crest using artificial neural network and support vector regression models. Soft Computing, 2019; 23: 9629–9645. doi:10.1007/s00500-018-3528-8.

[37] Qin, Y., Su, C., Chu, D., Zhang, J., Song, J. A Review of Application of Machine Learning in Storm Surge Problems. Journal of Marine Science and Engineering, 2023; 11: 1729. doi:10.3390/jmse11091729.

[38] Habib, M. A., Abolfathi, S., O'Sullivan, J. J., Salauddin, M. Efficient data-driven machine learning models for scour depth predictions at sloping sea defences. Frontiers in Built Environment, 2024; Volume 10 - 2024: doi:10.3389/fbuil.2024.1343398.

[39] Shah, S. A., Jehanzaib, M., Yoo, J., Hong, S., Kim, T.-W. Investigation of the Effects of Climate Variability, Anthropogenic Activities, and Climate Change on Streamflow Using Multi-Model Ensembles. Water, 2022; 14: 512. doi:10.3390/w14040512.

[40] Masoumi, F., Jorabloo, M., Shobeyri, G. Optimizing Reservoir Operations with Reinforcement Learning: A Data-Driven Framework. Civil Engineering and Applied Solutions, 2025; 1: 56–67. doi:10.22080/ceas.2025.29738.1032.

[41] Rodrigues, D. T., Santos e Silva, C. M., dos Reis, J. S., Palharini, R. S. A., Cabral Júnior, J. B., da Silva, H. J. F., Mutti, P. R., Bezerra, B. G., Gonçalves, W. A. Evaluation of the Integrated Multi-SatellitE Retrievals for the Global Precipitation Measurement (IMERG) Product in the São Francisco Basin (Brazil). Water, 2021; 13: 2714. doi:10.3390/w13192714.

[42] Židek, K., Piteľ, J., Balog, M., Hošovský, A., Hladký, V., Lazorík, P., Iakovets, A., Demčák, J. CNN Training Using 3D Virtual Models for Assisted Assembly with Mixed Reality and Collaborative Robots. Applied Sciences, 2021; 11: 4269. doi:10.3390/app11094269.

[43] Anderson, J. D., & Wendt, J. Computational fluid dynamics. ed. New York (NY): McGraw-hill; 1995.

[44] Hirt, C. W., Nichols, B. D. Volume of fluid (VOF) method for the dynamics of free boundaries. Journal of Computational Physics, 1981; 39: 201–225. doi:10.1016/0021-9991(81)90145-5.

[45] White, F. M., Majdalani, J. Viscous fluid flow. Fourth ed. New York (NY): McGraw-Hill; 2006.

[46] Santa Fe. Incorporated: FLOW-3D User's Manual Version 9.3. New Mexico (NM): 2008.

[47] Hirt, C. W., Sicilian, J. M. A porosity technique for the definition of obstacles in rectangular cell meshes. In: International Conference on Numerical Ship Hydrodynamics, 4th; 1985; Washington, DC (US). p. 19.

[48] Hirt, C. W. T. CFD-101: The Basics of Computational Fluid Dynamics Modeling, FLOW-3D Manual, Flow Science Press, Flow Science, Inc. 2011. https://www.flow3d.com/resources/cfd-101/.

[49] Meselhe, E., Hebert, K. Laboratory Measurements of Flow through Culverts. Journal of Hydraulic Engineering-asce - J HYDRAUL ENG-ASCE, 2007; 133: 973–976. doi:10.1061/(ASCE)0733-9429(2007)133:8(973).